39th AIAA/ASME/SAE/ASEE
Joint Propulsion Conference and Exhibit
July 20-23, 2003, Huntsville, AL

Paper 2003-4687

EXPERIMENTS STUDYING THERMAL CRACKING, CATALYTIC CRACKING, AND PRE-MIXED PARTIAL OXIDATION OF JP-10

M. Cooper and J.E. Shepherd
Graduate Aeronautical Laboratories,
California Institute of Technology, Pasadena, CA 91125

Practical air-breathing pulse detonation engines (PDE) will be based on storable liquid hydrocarbon fuels such as JP-10 or Jet A. However, without significant advances in initiation technology, such fuels are not optimal for PDE operation due to the high energy input required for direct initiation of a detonation and the long deflagration-to-detonation transition times associated with low-energy initiators. In an effort to utilize such conventional liquid fuels and still maintain the performance of the lighter and more sensitive hydrocarbon fuels, various fuel modification schemes such as thermal cracking, catalytic cracking, and partial oxidation have been investigated.

We have examined the decomposition of JP-10 through thermal and catalytic cracking mechanisms at elevated temperatures using a benchtop reactor system. The system has the capability to vaporize liquid fuel at precise flow rates while maintaining the flow path at elevated temperatures and pressures for extended periods of time. The catalytic cracking tests were completed utilizing common industrial zeolite catalysts installed in the reactor. A gas chromatograph with a capillary column and flame ionization detector, connected to the reactor output, is used to speciate the reaction products. The conversion rate and product compositions were determined as functions of the fuel metering rate, reactor temperature, system backpressure, and zeolite type.

An additional study was carried out to evaluate the feasibility of using pre-mixed rich combustion to partially oxidize JP-10. A mixture of partially oxidized products was initially obtained by rich combustion in JP-10 and air mixtures for equivalence ratios between 1 and 5. Following the first burn, air was added to the products, creating an equivalent stoichiometric mixture. A second burn was then carried out. Pressure histories and schlieren video images were recorded for both burns. The results were analyzed by comparing the peak and final pressures to idealized thermodynamic predictions.

Nomenclature

$Area_i$	area under detector signal for region i
f	number of carbon atoms in fictitious product compound
g	number of hydrogen atoms in fictitious product compound
m_{Ci}	mass of carbon atoms in region i
M_f	mass of liquid fuel injected into system
M_p	mass of products in system
n	normalized number of moles, $14/\phi$
n_1	number of moles before first burn
$n_{C,i}$	number of carbon atoms in region i
n_f	moles of liquid fuel injected into system
$(n_p)_1$	number of cooled moles of products from the first burn
n_p	moles of products in system
$P(t)$	instantaneous pressure of reactor panel
P_1	initial pressure before first burn
P_2	initial pressure before second burn
$(P_{max})_1$	maximum pressure of first burn
$(P_{max})_2$	maximum pressure of second burn
$(P_p)_1$	final pressure of cooled products after first burn
Q	heat release of mixture
$\tilde{R}$	universal gas constant
t	time
T	temperature

V	volume of combustion vessel
$V(t)$	instantaneous volume of reactor panel
$\mathcal{W}_f$	molecular weight of liquid fuel
$\mathcal{W}_p$	molecular weight of fictitious product compound
x_i	mole fraction of carbon atoms in region i
y	carbon mass fraction of all regions where $i \neq$ JP-10
y_i	carbon mass fraction in region i
ΔP	difference between maximum combustion pressure and initial pressure
ΔV_f	volume of liquid fuel injected into system
ϵ	effectiveness factor
γ	ratio of specific heats
ϕ	equivalence ratio
ρ_f	density of liquid fuel

Introduction

Pulse detonation engine (PDE) research has primarily been conducted with hydrocarbon fuels such as acetylene, ethylene, and hydrogen due to their ease of use in laboratory experiments. These light gaseous fuels have lower boiling points and reduced critical energies of initiation than storable liquid hydrocarbon fuels (i.e., JP-10 and Jet A) eliminating the need for high-energy ignition systems and heated test facilities. However, gaseous fuels require special storage and dispensing facilities which reduce the available payload capacity in addition to not meeting the engine cooling requirements for operation at supersonic flight speeds. Gaseous fuels also pose severe explosion hazards in comparison with liquids. For these reasons, liquid hydrocarbon fuels are essential for practical propulsion systems and special techniques of initiation or fuel modification will be needed in order to use these fuels in PDEs.

This paper presents the results of three studies that experimentally modify the JP-10 molecule in an effort to increase its sensitivity to detonation initiation. The modifications include hydrocarbon cracking of the parent JP-10 molecule into lower-molecular-weight hydrocarbons by thermal cracking at elevated temperatures and catalytic cracking with commercial zeolites. The tests are conducted in a benchtop reactor while product distributions are measured with a gas chromatograph. The mechanism of pre-mixed partial oxidation is tested in an explosion vessel. Pressure history measurements provided a measure of the effective energy content of the different mixtures tested. The results of the three studies have not been analyzed with respect to possible reaction mechanisms and pathways but rather to determine the feasibility of hydrocarbon cracking of JP-10 as a means of fuel sensitization for low-energy detonation initiation in PDEs.

Previous experimental work[1–3] has studied the detonation properties of a sensitized fuel containing additives such as methane, acetylene, ethers, and nitrates. Results of these studies found that additives are not an effective means of reducing the detonation sensitivity, and in some cases, were found to lengthen the time to detonation transition. Other means of reducing the critical ignition energy for PDE applications have included a separate driver section upstream of the main detonation tube. Under the correct conditions, a separate driver has enabled less sensitive mixtures to detonate; however, this method does not eliminate the need for a sensitive gaseous fuel and oxidizer. Thus, the additional payload capacity gained by using the storable liquid hydrocarbon fuels is reduced. If JP-10 is to be used directly in hypersonic flight, temperatures are expected to be near or above the auto-ignition temperature of the fuel. Zhang et al.[4] completed detonation studies of JP-10 vapor detonation near the auto-ignition temperature observing a significant increase in cell size with a corresponding increase in the initiation energy. An alternative to pre-initiator systems is chemical modification of the fuel producing a mixture of molecules that are smaller than the parent molecule and, hopefully, easier to detonate.

Why study JP-10?

We study JP-10 (Fig. 1) because it is a popular missile fuel due to its increased energy storage through strained cyclic geometries[5] and is considered ideal for volume-limited applications.[6] Because JP-10 is a single-component hydrocarbon, results of testing with the neat fuel is less variable than tests with other kerosene-based fuels in which their composition is based only on specifications on boiling range, vapor pressure, contaminants, and freezing point such as RP-1, Jet A, or JP-5,7,8.[7] Little is known of JP-

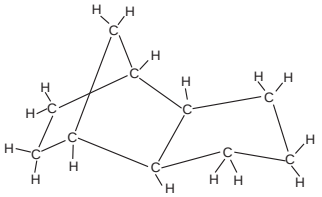

Fig. 1 Structure of JP-10 ($C_{10}H_{16}$) molecule.

10's high temperature chemistry since few experiments identifying the hydrocarbon cracking mechanisms have been completed. However, experiments on detonation pressure, detonation wave speed, and cell width have been completed in JP-10 mixtures and mixtures representative of decomposed JP-10.[1] Both the high initiation energy and large cell size characteristic of JP-10 mixtures indicate low mixture sensitivity to detonation initiation. JP-10 does have a similar cell size to propane (Fig. 2) with similar difficulties in initiation. Schauer et al.[8] have achieved detonations in

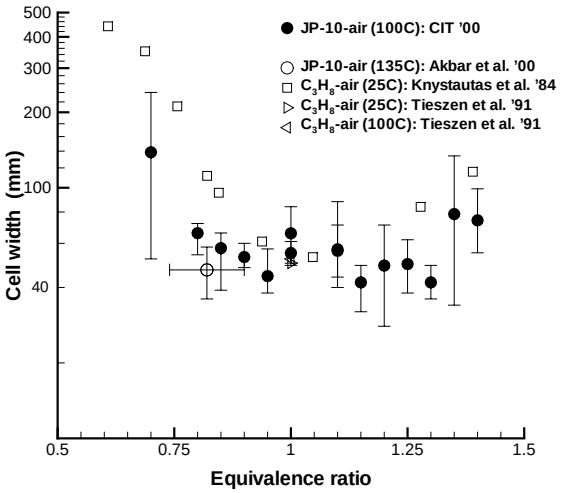

Fig. 2 Cell widths of JP-10 and propane mixtures as a function of equivalence ratio.

propane-air mixtures, but only for a limited range of equivalence ratios.

Benchtop reactor facility

A benchtop reactor facility, consisting of a "reactor panel" and a gas chromatograph (GC), was constructed for the thermal and catalytic cracking experiments (Fig. 3).

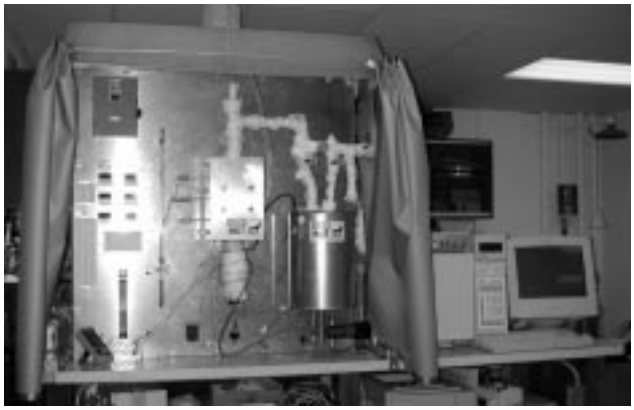

Fig. 3 Photograph of reactor panel with gas chromatograph.

The flow path of the JP-10 fuel is better illustrated in the schematic of Fig. 4. The liquid JP-10, initially contained in the buret, is pumped into the evaporator by a fuel pump through the fuel inlet valve (FIV). The fuel pump is a precision metering pump capable of flow rates between 0.025 and 1.5 ml/min. A backpressure on the pump of at least 5 kPa is required to prevent flow-through, so the system is initially pressurized by industrial nitrogen via the gas inlet valve (GIV). The evaporator consists of a 200-ml cylindrical vessel with Swagelok fittings welded to the top and bottom end flanges and is heated to 270±2°C for vaporization of

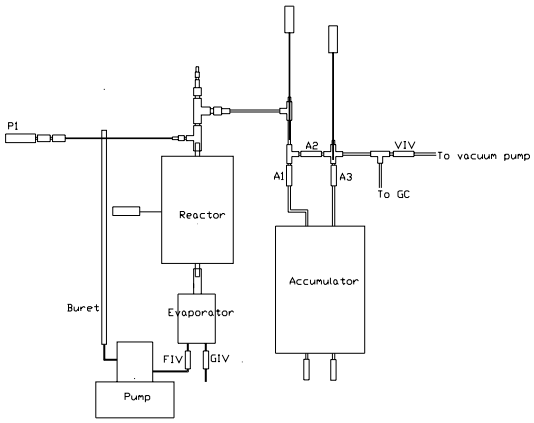

Fig. 4 Schematic of reactor panel with main components labeled.

the fuel which then travels into a temperature controlled reactor. Within this reactor, the fuel will come into contact with the zeolite catalyst, if installed, and be cracked into lower-molecular-weight hydrocarbons. The reactor contains a 1/2-inch diameter stainless steel tube encased by two copper blocks . Cartridge heaters embedded in the copper blocks allowed operation up to 500±2°C. A pressure gauge, labeled as P1 on Fig. 4, is located at the reactor outlet. Upon exiting the reactor, the products flow through the outlet plumbing and enter the heated accumulator from which samples are taken by the GC.

The accumulator consists of a stainless steel vessel that can change its volume through an internal piston to a maximum of 1875±1 cc. It is heated to 230±10°C. Orientation of the upstream needle valves (A1, A2, and A3 of Fig. 4) allow the accumulator to be operated in a filling or emptying mode. In the filling mode, all flow from the reactor is directed into the accumulator. In the emptying mode, all flow is directed out of the accumulator to the GC. A constant backpressure may be supplied to the bottom of the accumulator piston by adjusting a venting regulator supplied with industrial air.

All connections between the main panel components were heated to a nominal temperature of 200±10°C with rope heaters and made with stainless steel tubing and Swagelok connectors. The heated components and associated connections were grouped into four heating zones, each with a dedicated temperature controller. A vacuum pump was attached to the system outlet in parallel with the GC and downstream of the vacuum isolation valve (VIV). Refer to Cooper and Shepherd[9] for additional specifics of the experimental facility.

Gas chromatography

A capillary GC (Agilent 6890 Series) was connected to the reactor panel outlet for product component analysis. The capillary column has a stationary phase of HP-5 (crosslinked 5% Phenyl Methyl Siloxane) with dimensions of 30 m × 0.32 mm × 0.25 μm. The carrier

gas was ultra-high-purity helium and a flame ionization detector (FID) quantified the column effluent.

Samples from the accumulator were taken by a 0.25-ml sampling loop and the pneumatic, gas sampling valve of the GC. Due to the size of our reactor panel and associated tubing, sample injections were often too large resulting in column saturation and non-optimal GC operation. In an effort to reduce the sample size and prevent column saturation, the inlet split ratio was set to the maximum value of 400:1 at an inlet temperature of 250°C. The column flow was 2 ml/min. Because of the low conversion of the parent molecule into product species, the column continued to be saturated with JP-10 during each test. To promote component separation and ordering of the elution times by each component boiling temperature, an oven program of hold for 3 minutes at 30°C, ramp to 200°C at a rate of 10°C/min and hold at 200°C for 3 minutes was used in each analysis. Residual hydrocarbon, especially JP-10, in the stainless steel plumbing was observed and found to be difficult to flush from the system between each test.

Initial GC testing yielded retention times for the alkanes between C_5 and C_{12} in addition to JP-10 and found that they were ordered by their boiling temperature as expected (Fig. 5). Boundaries defining regions

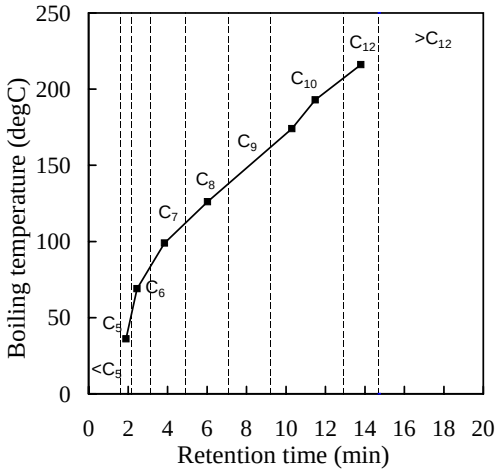

Fig. 5 Boiling temperature of alkanes and JP-10 versus measured retention times with region boundaries.

in which compounds with the same carbon number are expected to elute from the column also appear in Fig. 5. Woodrow[10] used this technique as a means of quantifying the composition of Jet A vapor since detailed component analysis is not possible with a FID. The FID signal is proportional to the number of carbon atoms eluting at a given time. By integrating this signal over a range of retention times, the resulting area $Area_i$ under the FID signal is proportional to the number of carbon atoms $n_{C,i}$ in that region.

$$Area_i \propto n_{C,i} \tag{1}$$

The areas assigned to retention times in each region are summed. The summed areas in each region are divided by the summed areas in all regions,

$$\frac{Area_i}{\sum_i Area_i} \propto \frac{n_{C,i}}{\sum_i n_{C,i}} = x_i \ , \tag{2}$$

resulting in an associated mole fraction x_i of *carbon atoms* for each region of FID signal integration. Since the FID determines only the number of carbon atoms, this is also the mass fraction y_i for that region.

$$y_i = \frac{m_{C,i}}{\sum_i m_{C,i}} = \frac{12 \text{ g/mol} \cdot \text{n}_{\text{C,i}}}{\sum_i 12 \text{ g/mol} \cdot \text{n}_{\text{C,i}}} = x_i \tag{3}$$

The resulting *carbon* mass fraction is what is being reported in the subsequent sections of this report. We report this instead of number density or mass fraction of a particular species since we do not know exactly what species are being eluted. Speciation would require further analysis by a GC/MS. Although we have calibrated the retention times with pure hydrocarbon test species, the actual reactor products will involve species other than those used for calibration.

Reactor product species are not assured to be ordered in terms of the carbon number in exactly the same fashion as the calibration species. Reducing the FID output in terms of carbon mass instead of species amount eliminates possible over or under counting of species in this situation. The ratio of hydrogen to carbon is also not known for the reactor products. While this makes only a modest difference in determining the molar mass, it prevents us from precisely determining the mass fraction on a species basis. Since C is 12 times heavier than H, as long as the H/C ratio does not vary too wildly, then the carbon mass ratio distribution will be similar to the actual species mass distribution.

In conclusion, without a great deal of further analysis, what the FID reports is proportional to the mass of carbon atoms. The data reduction does not account for the hydrogens and the reported mass fraction y_i is strictly on a carbon-only basis.

Experimental procedure and data reduction methods

After heating the system to the desired operating temperatures as described above and in more detail in Cooper and Shepherd,[9] the system was evacuated and subsequently filled with nitrogen to a pressure slightly above atmosphere to obtain the required backpressure on the fuel pump. The FIV was opened, the accumulator was set to filling mode, and the test was started by turning on the fuel pump. At regular time intervals, the elapsed time, buret liquid level, system pressure, and accumulator position were recorded.

A volume of 4.8±0.4 ml of JP-10 was injected during each thermal and catalytic test. Approximately 1.0±0.2 grams of zeolite was installed for the catalytic

cracking tests. These values were calculated based on experiments by Lopes et al.[11] who used a WHSY (weight of component per hour per unit weight of zeolite) value equal to 6.9 hr^{-1}. The inverse of this value is referred to as the "time on stream". Assuming one gram of zeolite is installed in our system, the fuel flow rate of 10.6 g/hr corresponds to a time on stream of approximately 330 s, and the fuel flow rate of 2.3 g/hr corresponds to a time on stream of approximately 1570 s. These time on stream values are similar to other documented experiments.[12–15] The zeolite catalyst was observed to coke significantly during a single test so that fresh catalyst was installed before each test.

After injecting the desired amount of JP-10, the fuel pump was shut off and the FIV closed. A baseline run was conducted with the GC by taking a gas sample from the evacuated plumbing between the GC and valve A3 (as labeled in Fig. 4). The accumulator was set to emptying mode and valve A3 was held open allowing the products to flow through the sample loop. The GC sampling valve was cycled capturing a volume of the accumulator products for analysis. This GC sampling procedure was completed three times for most of the tests. Because of the run time determined by the oven program and subsequent cool down, samples from the accumulator were taken approximately 45 minutes apart. The baseline GC samples have been subtracted from the samples of the accumulator products.

Mole balance calculations

The moles of liquid fuel injected were compared to the moles of product created and we refer to these calculations as a mole balance. When JP-10 cracks into lower-molecular-weight components through the different mechanisms of hydrocarbon cracking, the number of product moles will increase. From the buret liquid level, system pressure, and accumulator position recorded during each test, the injected and product moles are calculated.

As fuel is injected into the system, the buret liquid level changes over time by an amount ΔV_f. The mass, $M_f = \Delta V_f \cdot \rho_f$, and moles, $n_f = M_f/\mathcal{W}_f$, of the injected fuel can be calculated with the known fuel density ρ_f and molecular weight $\mathcal{W}_f$ of liquid JP-10.

The moles of products in the system can be calculated with the ideal gas law (Eq. 4) given the instantaneous system pressure $P(t)$ and volume $V(t)$ along with the nominal system temperature T of 473 K. The instantaneous system volume is calculated from the accumulator position recorded at regular time intervals.

$$n_p = \frac{P(t) \cdot V(t)}{\tilde{R} \cdot T} \tag{4}$$

A single figure illustrating the mole balance is obtained by plotting the moles of products created n_p as a function of the moles injected into the system n_f. The slope of this line is the mole ratio, n_p/n_f, and is used as a key diagnostic in our tests. In our plots that follow, the solid line with $n_p/n_f = 1$ refers to the case of "zero conversion" of the fuel into lower molecular weight components. If there is a net mole increase due to reaction, the slope of the line is greater than one, $n_p/n_f > 1$. For a given liquid fuel flow rate, the accumulator volume increases more rapidly with time for a higher molar conversion ratio.

Mass balance calculations

While complete conversion of JP-10 to products was assumed in the mole balance calculations above, the actual conversion is usually quite incomplete and only a fraction y of the original mass of fuel is converted. The amount of JP-10 converted can be measured with the GC by determining the fraction of carbon mass in all the species other than JP-10. Using the notation of equation 3, the carbon mass fraction of species region i is y_i and the conversion mass fraction is

$$y = \sum_{i \neq \mathrm{JP10}} y_i = \frac{\sum_{i \neq \mathrm{JP10}} Area_i}{\sum_i Area_i} \tag{5}$$

which we express as %wt conversion ($100 \times y$).

The mass conversion can be related to the mole ratio discussed previously by considering the mass balance for the processes in the reactor. The sequence of events in the reactor can be idealized as liquid injection, vaporization, reaction in the catalyst bed, and storage in the accumulator. The partial reaction of n_f moles of JP-10 vapor can be represented schematically as

$$\begin{aligned} n_f \mathrm{C_{10}H_{16}} \longrightarrow\ & n_f(1-y)\mathrm{C_{10}H_{16}} \\ & + (n_p - n_f(1-y))\,\mathrm{Products}\ . \end{aligned} \tag{6}$$

The hydrocarbon "Products" represent a notational species that has the average molar mass of the actual products and fictitious composition $\mathrm{C}_f\mathrm{H}_g$ appropriate to the mixture. The products have an average molar mass of $\mathcal{W}_p = 12f + g$, where f and g represent an empirical composition appropriate to the mixture and are not necessarily integers. If all of the product species are correctly accounted for, then the hydrogen-to-carbon ratio f/g must equal 1.6 if we consider that the JP-10 either reacts or remains in the original state. GC measurements indicate that this appears to be the case.

From the reaction equation 6, the mass balance will be

$$\begin{aligned} M_f &= n_f \mathcal{W}_f \\ &= n_f(1-y)\mathcal{W}_f + (n_p - n_f(1-y))\,\mathcal{W}_p\ . \end{aligned} \tag{7}$$

This can be simplified to

$$\frac{\mathcal{W}_p}{\mathcal{W}_f} = \frac{y}{n_p/n_f - (1-y)}\ . \tag{8}$$

This is the key relationship between mass conversion y, mole conversion n_p/n_f, and the average product molar mass $\mathcal{W}_p$. Using values of the mass and mole conversion obtained from the experiments enables us to predict the average product molar mass. Another way to look at this is as a relationship between molar conversion ratio and mass conversion fraction for a fixed average molar mass of the products.

$$\frac{n_p}{n_f} = 1 + \left(\frac{\mathcal{W}_f}{\mathcal{W}_p} - 1\right) y \tag{9}$$

Using this version of the relationship, the expected molar ratio can be predicted as a function of product molar mass and conversion ratio. The limiting cases are: no conversion, $y = 0$ and $n_p/n_f = 1$; complete conversion, $y = 1$ and $n_p/n_f = \mathcal{W}_f/\mathcal{W}_p$.

Thermal decomposition

Two studies have been completed previously investigating the thermal breakdown of JP-10. Green et al.[16] studied JP-10 pyrolysis in a flowing reactor with residence times of approximately 2 ms and temperatures up to 1500 K where a heated quartz tube was used eliminating the possibility of surface reactions. Product analysis with a GC-MS observed benzene at temperatures greater than 1250 K and cyclopentadiene below 1250 K.[16] Davidson et al.[5] investigated JP-10 pyrolysis behind a reflected shock at conditions between 1.2 to 1.5 bar and 1100 to 1700 K. The UV absorption cross-sections of the decomposition products did not show any benzene. This is possibly due to the short test time ($\sim$50 μs) since benzene is expected to form through secondary chemical reactions at later times.[5] We conducted thermal cracking experiments in the benchtop reactor with a maximum reactor temperature of 500°C to determine the amount of conversion of JP-10 into lower-molecular-weight species. Selected results are presented below to illustrate the major conclusions. The results for all of the individual tests can be found in their entirety in Cooper and Shepherd.[9]

Results

The first tests investigated the effect of liquid fuel flow rate. Tests were conducted with liquid fuel flow rates of 2.3 g/hr, 6.2 g/hr, and 10.6 g/hr. Graphs of the calculated moles of product (based on instantaneous system temperature and pressure with Eq. 4) versus the injected moles of liquid fuel appear in Fig. 6, 7, and 8. In each graph, the solid line represents the case of zero conversion and the dotted line represents the average of the experimental data at that flow rate.

The slope of these mole balances, called the mole ratio, corresponds to the number of moles of products divided by the number of moles of JP-10 injected into the system (Fig. 9). There is substantial scatter in this

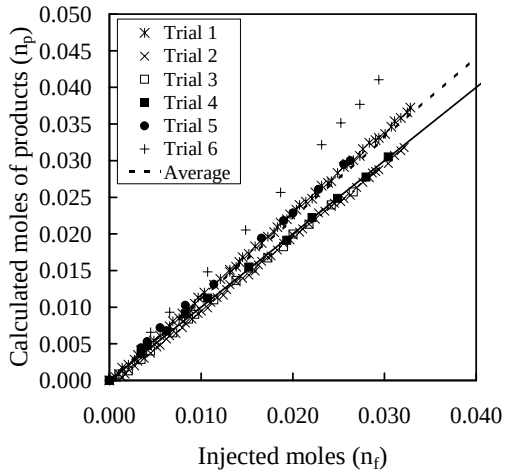

Fig. 6 Comparison of moles of products to moles of injected JP-10 for thermal decomposition tests with a liquid fuel flow rate of 2.3 g/hr.

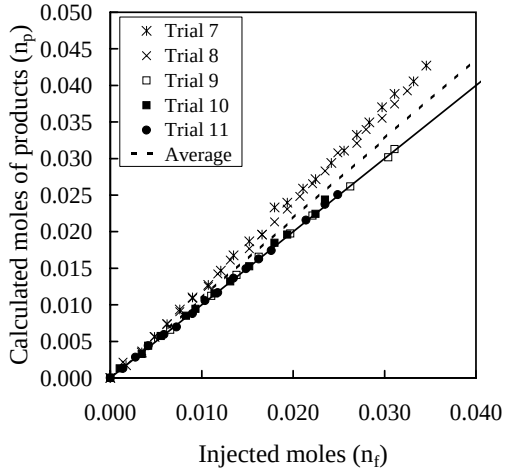

Fig. 7 Comparison of moles of products to moles of injected JP-10 for thermal decomposition tests with a liquid fuel flow rate of 6.2 g/hr.

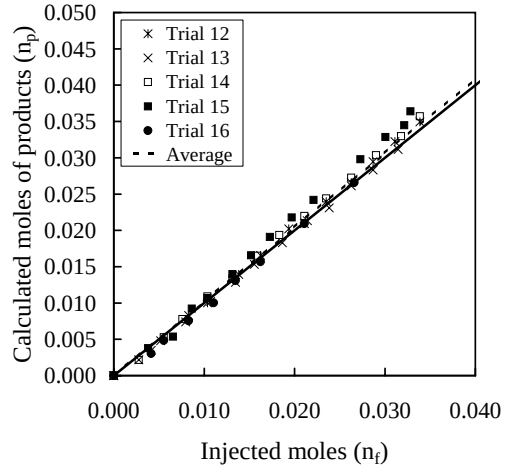

Fig. 8 Comparison of moles of products to moles of injected JP-10 for thermal decomposition tests with a liquid fuel flow rate of 10.6 g/hr.

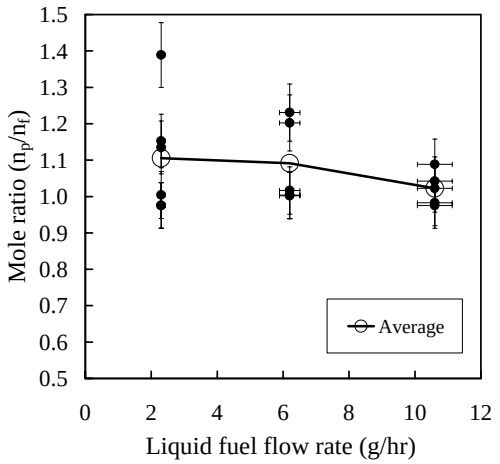

Fig. 9 Mole ratio data for each thermal decomposition test at the different liquid fuel flow rates. Straight line represents the average mole ratio.

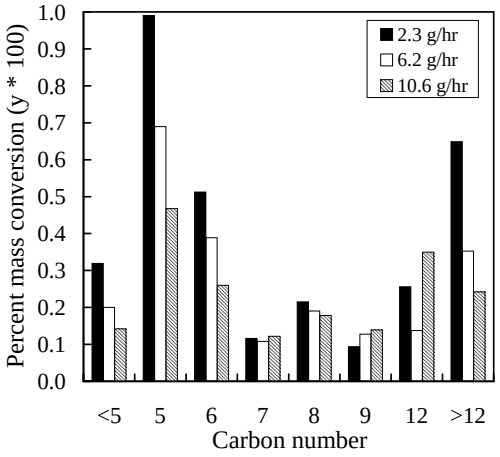

Fig. 10 Overall product composition for thermal decomposition tests averaged over individual tests at the same liquid fuel flow rate and multiple GC samples. C_{10} species are omitted for clarity.

plot for the lowest flow rate (2.3 g/hr), where the mole ratios varied between 0.975 and 1.389. The scatter decreases for the intermediate flow rate (6.2 g/hr) and is minimal for the highest flow rate (10.6 g/hr). The reasons for the scatter at low flow rates is not obvious but the condition of the stainless steel tubing and fittings used for the reactor channel and plumbing are the obvious factors. It is known[15,17] that stainless steel can exhibit catalytic activity and the effectiveness of this action will depend strongly on the surface condition of the steel. No attempt was made to control the surface condition in the present tests because that would have been very difficult to do in any case. The reactor plumbing was also very difficult to clean out, as mentioned previously, since the fittings contained many crevices that can trap fuel or decomposition products. Finally, in some tests, the total motion of the tell-tale on the accumulator was extremely small and the instantantous measurement of the system volume was subject to significant uncertainty.

Multiple GC samples were generally taken from the accumulator and were averaged enabling a direct comparison of the effect of fuel flow rate on the product species distribution (Fig. 10). The percent conversion of JP-10 into products of lower molecular weight, as determined from the GC output, increases as the flow rate decreases (Table 1).

Fuel flow rate (g/hr)	mole ratio	% conversion
2.3	1.11	3.15
6.2	1.09	2.19
10.6	1.02	1.90

Table 1 Major results of thermal cracking tests. Overall average percent conversion of JP-10 and mole ratio for the different fuel flow rates.

Despite the variability, the cases at the two higher flow rates yielded average molar conversion ratios between 1.02 and 1.09 (Fig. 10) and mass conversion amounts of less than 3% (Table 1). Reducing the liquid fuel flow rate from 10.6 g/hr to 2.3 g/hr resulted in increasing the average mass conversion up to 6% in the most extreme case.[9] The variability in the mass conversion ratios is probably associated with the difficulty in flushing the JP-10 from the system between runs and the saturation of the column and detector due to the very high concentration of JP-10.

The mole ratio is plotted as a function of the mass conversion fraction in Fig. 11. Clearly, the conversion

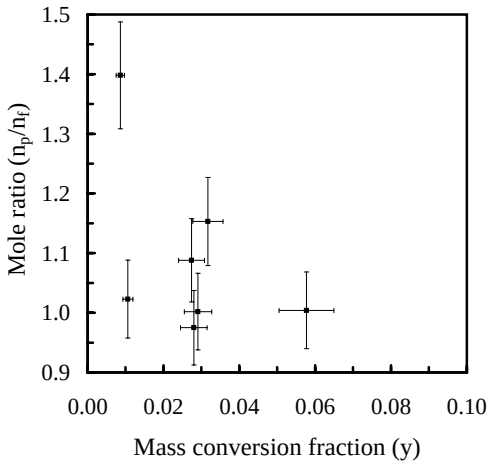

Fig. 11 Observed mole ratio n_p/n_f as a function of the mass conversion fraction y for the thermal decomposition tests.

amounts and the molar ratios have too much variability to draw any conclusions about an average molar mass of the products. However, it can be seen through these results that thermal decomposition of JP-10 at a temperature of 500°C is not sufficient to promote adequate chemical breakdown. Converting at best 3% of the mass of JP-10 to lighter-weight compounds is unlikely to increase the fuel's sensitivity to detonation.[1]

Catalytic cracking

We investigate the use of a catalyst to accelerate the C-C bond fission reactions and increase the production of lower-molecular-weight components in the following experiments. The catalysts consisted of a porous, crystalline alumniosilicate of a specific molecular structure referred to as a zeolite. Commercial processes that produce gasoline and high grade military fuels from crude oils typically use fluidized bed reactors containing a mixture of zeolite catalyst and crude oil.[18,19] Zeolite catalysts used in these harsh operating conditions of heavy oil cracking are typically of the faujausite (FAU) structure.[19] The HY zeolite studied here has the FAU structure.

Because of the shared oxygen atoms between the AlO_4 and SiO_4 tetrahedrals, the zeolite framework possesses a net negative charge which is balanced by the addition of protons. After proton addition, the zeolite becomes a strong Bronsted acid containing sites for hydrocarbon adsorption.[20] The number density and orientation of these active sites depend on the channel and cage dimensions as defined by the zeolites framework and can influence shape-selectivity of the cracking products. Molecules with dimensions larger than the zeolite pore dimensions typically can not enter the channels and obtain access to the internal active sites, but there are exceptions to this statement. Pore diameters of several common zeolite structures appear in Table 2. It is important to note that these dimensions can vary slightly depending on the zeolite's hydration state and temperature.[21] FAU zeolites are commonly referred to as "large pore" zeolites because they have supercages approximately 13 Å in diameter which can accommodate large components.[22] Beta is an additional zeolite structure; however, there are few documented experiments using Beta to catalytically crack hydrocarbons.

Zeolite	Pore Diameter (Å)
Faujasite (FAU)	7.4
Beta (BEA)	7.6 to 5.5
ZSM-5 (MFI)	5.1-5.6

Table 2 Pore diameters of common zeolites.

The FAU and ZSM-5 zeolites have been found to deactivate quickly in reactions with hydrocarbons as a result of coke deposition.[20,22] In an effort to create a zeolite that is more coke resistant, an ultra-stable form of zeolite Y (USY) was created. USY is known to produce more olefins due to decreased hydrogen transfer reactions, produce more aromatics due to a reduction in coke formation, and have a higher thermal stability than HY.[18] Additional attempts to reduce the coking tendency through structural improvements to the FAU structure have met with little success.[23,24]

A variety of studies have been completed with these zeolites. For example, normal alkanes[11,14,20,24,25] and heavy oils[23] have been studied extensively to characterize zeolite cracking properties in catalytic reforming reactions. Few studies[13,26,27] have investigated the cracking of JP-10 with zeolites. Additional studies[17,26–28] have investigated the thermal and catalytic cracking of other liquid hydrocarbon fuels. In particular, some studies determined the fuel endothermicity for supersonic engine cooling applications[17,26,27] while others investigated the factors that affect deposit formation on the zeolite itself.[13,29]

Typically, the catalytic cracking results are corrected for the products generated due to the thermal cracking reactions. However, because the thermal cracking reactions in our experiments resulted in less than 3% conversion, we do not attempt to correct our catalytic cracking data.

Zeolite preparation

The zeolite Y powder with a Si/Al ratio (SAR) of 6.0 was obtained in sodium form. It was protonated by ion exchange with 1 M solution of aluminum nitrate at a ratio of 1 g of zeolite to 0.1 l of solution and allowed to stir for at least 12 hours. The zeolite was then filtered from the solution, a new solution made, and the zeolite returned to the flask for another 12 hours of mixing. This process was repeated 4 times.

After the fourth filtration, the zeolite powder was calcined in a temperature controlled oven under flowing dry nitrogen. The oven temperature was increased at a rate of 5°C/min from 30 to 250°C, held at 250°C for 4 hrs, and then increased at the same rate to a temperature of 500°C. It was held at this temperature for approximately 6 hrs.

The zeolite powder was formed into pellets by compressing the powder and sifting through two meshes of sizes #60 and #45. The pellets on the #60 mesh were saved for installation into the reactor.

When the zeolite became coked, the active sites were regenerated by heating the coked zeolite in an oven with flowing dry nitrogen as the temperature was increased from 30 to 200°C at a rate of 1°C/min. It was held at 200°C for 3 hrs. Then the nitrogen supply was turned off and the air supply turned on. The temperature was increased again at the same rate to 550°C then allowed to cool to room temperature in the air environment.

After installing the zeolite within the reactor tube, the reactor temperature was increased in a manner as to prevent destruction of the zeolite framework and to evaporate the absorbed water from the active sites. Under flowing nitrogen through the GIV of the reactor panel, the reactor temperature was ramped at a rate of 2.7°C/min from room temperature to 250°C and held at this temperature for 4 hours. A second temperature increase at the same rate to the desired reactor operating temperature (250, 300, 350, 425, or 500°C) followed.

Results

Effect of zeolite activity

The catalyst was found to become coked after a single test at the nominal test conditions of approximately 4.8 ml of JP-10 injected and a reactor temperature of 500°C. Thus, each test began by replacing the mass of coked zeolite pellets with those containing active sites. The active zeolites came from two batches (Fig. 12) prepared during the duration of the testing in addition to regeneration of the first batch (Fig. 13). Since the zeolite activity was not verified by standard

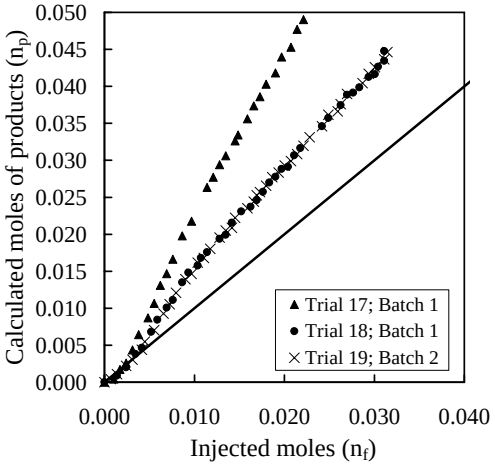

Fig. 12 Comparison of moles of product to moles of injected JP-10 from tests with the first and second batches of HY zeolite. Fuel flow rate is 2.3 g/hr. Reactor temperature was 500°C.

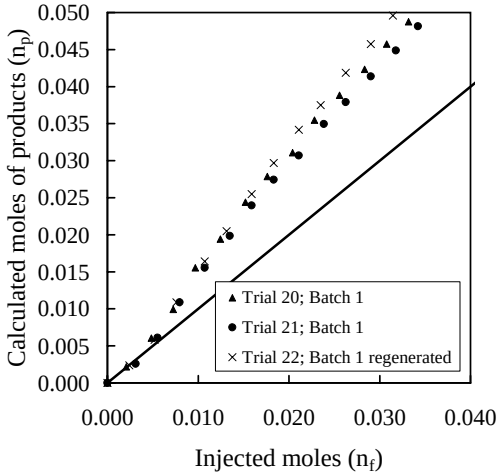

Fig. 13 Comparison of moles of product to moles of injected JP-10 from tests with the first and second batches of HY zeolite. Fuel flow rate is 10.6 g/hr. Reactor temperature was 500°C.

tests before installation, the conversion ratios provided the only available means with which to verify similar zeolite activity. The activity as measured by the mole balance seemed to be more consistent than the GC percent conversion (Table 3).

		1st batch	1st batch regenerated	2nd batch
2.3 g/hr	mole ratio:	1.83	-	1.44
	% conv.:	34	-	36
10.6 g/hr	mole ratio:	1.47	1.58	-
	% conv.:	31	61	-

Table 3 Effect of zeolite activity on conversion.

The procedure described above could be used to successfully regenerate the zeolite activity. The ratio of product moles to injected moles was measured to be an average of 1.47 and 1.58 for the original and regenerated batches, respectively. The number of times the same zeolite pellets may be regenerated and still maintain high activity should be further investigated. The regeneration process is a useful means to restore zeolite activity but, over time, the molecular structure can degrade. Because of the significant coking observed in our tests, a higher regeneration temperature than values used in the heavy oil cracking industry was required. Holding the zeolite within this high temperature environment acts to accelerate the structural degradation of the zeolite.

Effect of liquid fuel flow rate

To compare the effect of liquid fuel flow rate on conversion, the data of Fig. 12 and Fig. 13 with HY zeolite at a reactor temperature of 500°C were averaged. An overall average mole ratio of 1.70 and 1.51 for a flow rate of 2.3 g/hr and 10.6 g/hr, respectively, was calculated (Fig. 14). Thus, 11.3% more moles of products were produced at the lower flow rate.

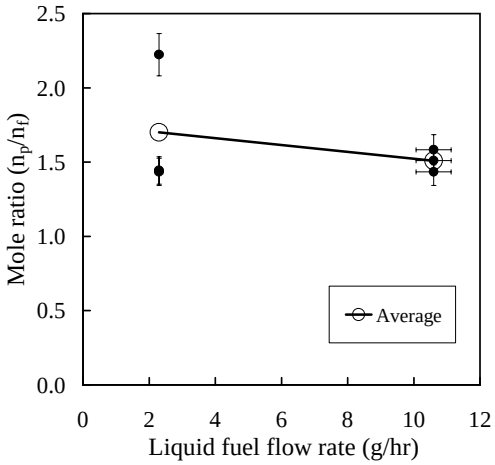

Fig. 14 Mole ratio data for tests with HY zeolite. The average ratio is denoted by a straight line.

The average product composition considering multiple GC samples for the above tests with HY zeolite at a reactor temperature of 500°C appears in Fig. 15. The variation in composition is slight with the lower fuel flow rate increasing the percent weight of the C_5 components approximately 2% and decreasing the coking products ($>C_{10}$) by a total of 9%. These large carbon

number compounds are indicative of coke and coke precursors. The formation of these deposits is known to be accelerated at higher flow rates which correspond to higher Reynolds numbers.[13,29] This agrees with our results. The overall average conversion of JP-10 with the HY zeolite at a fuel flow rate of 2.3 g/hr is 34% while the overall average conversion at a fuel flow rate of 10.6 g/hr is 41% (Table 4).

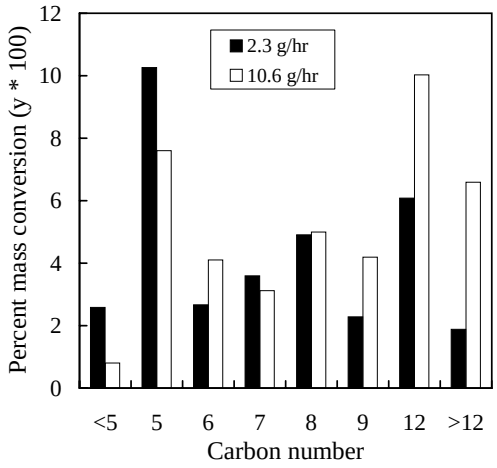

Fig. 15 Averaged product composition as a function of liquid fuel flow rate for HY zeolite. The C_{10} species are omitted for clarity.

Fuel flow rate (g/hr)	mole ratio	% conversion
2.3	1.70	34
10.6	1.51	41

Table 4 Effect of fuel flow rate on catalytic cracking tests with HY zeolite at a reactor temperature of 500°C.

Effect of zeolite type

Zeolites Beta and ultrastable-Y (USY) were also tested in addition to HY at the nominal reactor conditions of 500°C and a fuel flow rate of 2.3 g/hr. A single test was conducted with each zeolite and the mole balance results are compared with the overall average HY data at the same fuel flow rate (Fig. 16). The USY had a much lower activity observed by a mole ratio of 1.14. The Beta and HY zeolites had similar activities as observed by mole ratios of 1.67 and 1.70, respectively. It should be noted that the pore diameters of HY and Beta (Table 2) are similar so comparable conversion of JP-10 into other compounds is expected.

The multiple GC samples for each test are averaged and compared to the average product distribution of HY (Fig. 17). The overall average percent mass conversion of JP-10 was 70% for Beta and 11% for USY (Table 5). These are compared with the overall average conversion of HY at the same fuel flow rate of 34%. Beta has a greater relative percentage of C_5 components whereas USY has a greater relative percentage of C_6 compounds. Since USY cracks the JP-10 into

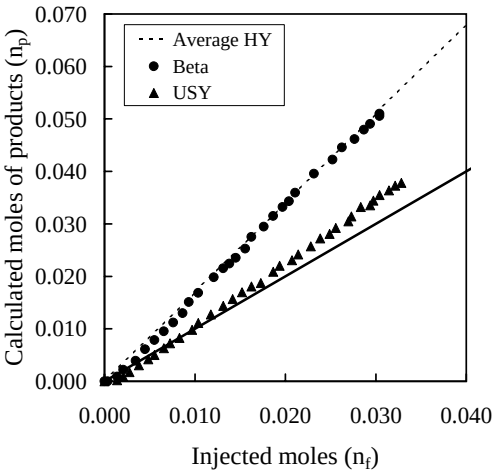

Fig. 16 Comparison of moles of products to moles of injected JP-10 for tests with different zeolites.

larger compounds as compared with HY and Beta, the decreased conversion observed is not surprising.

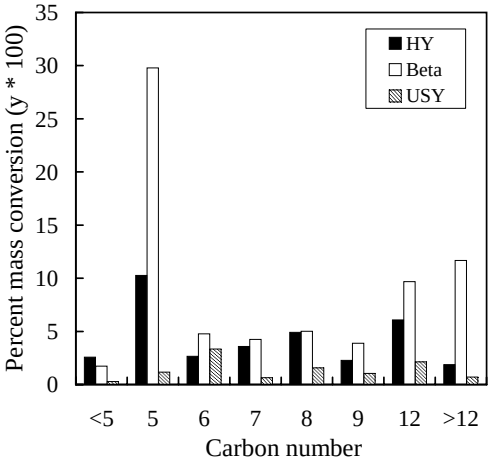

Fig. 17 Average product composition comparing different zeolites at a fuel flow rate of 2.3 g/hr. The C_{10} species are omitted for clarity.

Zeolite	mole ratio	% conversion
HY	1.70	34
USY	1.14	11
Beta	1.67	70

Table 5 Effect of zeolite type on catalytic cracking tests at a reactor temperature of 500°C and fuel flow rate of 2.3 g/hr.

Comparison of catalytic and thermal cracking

The mole ratio increases from 1.11 to 1.70 at a flow rate of 2.3 g/hr and it increases from 1.02 to 1.51 at a flow rate of 10.6 g/hr when the catalyst is installed in the reactor (Table 6). A comparison of the overall average product compositions appears in Fig. 18 for a flow rate of 2.3 g/hr and Fig. 19 for a flow rate of 10.6 g/hr. The catalytic tests increase the conversion of JP-10 as expected, with increased amounts of the

		Thermal	Catalytic
2.3 g/hr	mole ratio:	1.11	1.70
	% conv.:	3.15	34
10.6 g/hr	mole ratio:	1.02	1.51
	% conv.:	1.90	41

Table 6 Effect of catalytic and thermal cracking on conversion.

smaller carbon components, particularly the C_5 components.

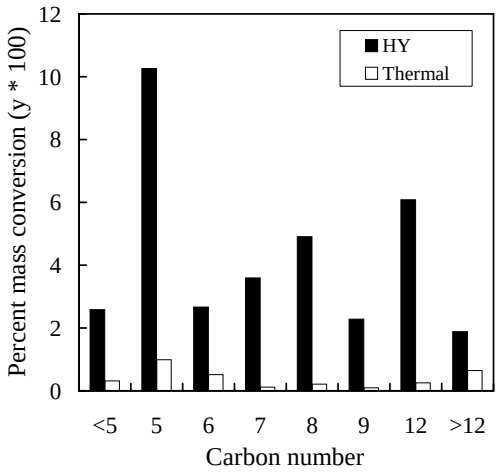

Fig. 18 Overall average product distributions for tests with and without catalyst installed in the reactor at a fuel flow rate of 2.3 g/hr. The C_{10} species are omitted for clarity.

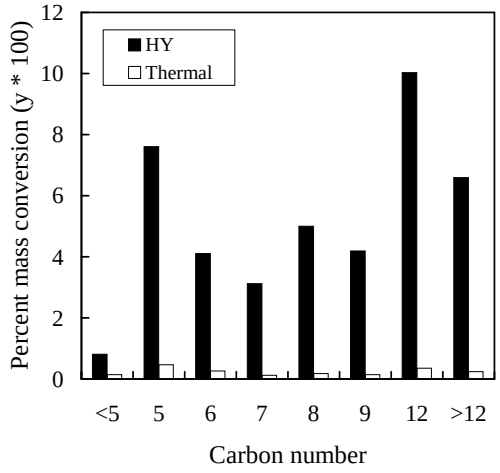

Fig. 19 Overall average product distributions for tests with and without catalyst installed in the reactor at a fuel flow rate of 10.6 g/hr. The C_{10} species are omitted for clarity.

Effect of pressure

The effect of system pressure was also studied at a liquid fuel flow rate of 10.6 g/hr. The system was pressurized to 400 kPa of nitrogen before the FIV was opened or the fuel pump turned on. The bottom of the accumulator was also pressurized to 400 kPa with air. Due to the increased pressure, the piston movement was reduced resulting in increased uncertainty in the gauge reading as compared with the baseline tests. This is observed through a slight increase in the data point scatter of the mole balance results (Fig. 20). The data are plotted with the overall average HY mole balance. The ratio of product moles to injected moles at the higher system pressure is 1.00 which is similar to the average mole ratio of 1.10 obtained by the thermal hydrocarbon cracking reactions.

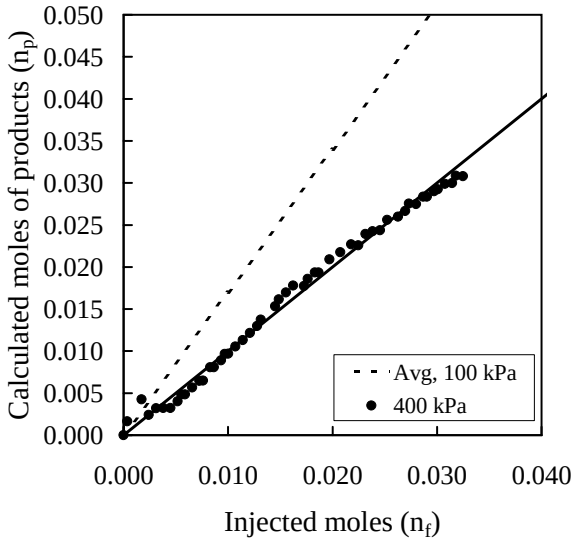

Fig. 20 Comparison of moles of product to moles of injected JP-10 in a system with HY zeolite at different system pressures. Fuel flow rate is 2.3 g/hr.

A look at the average product distribution from multiple GC samples (Fig. 21) yields a significant fraction of products with carbon numbers greater than 10. Thus, the higher pressure inhibits the cracking reactions that produce lower-molecular-weight compounds and enhances coking. This is expected because the higher pressure acts to increase the Reynolds number which is known to increase deposit formation.[13,29] Additionally, by Le Chatlier's principle, an increase in the pressure would cause the chemical reactions to proceed in a manner decreasing the number of moles in the system. Thus, higher-molecular-weight species would be formed. The overall average conversion at a system pressure of 400 kPa is 53% versus the conversion at atmospheric pressure of 34% (Table 7).

Pressure (kPa)	mole ratio	% conversion
100	1.70	34
400	1.00	53

Table 7 Effect of system pressure on catalytic cracking tests with HY zeolite at a reactor temperature of 500°C and a fuel flow rate of 10.6 g/hr.

Effect of reactor temperature

The effect of reactor temperature was studied with HY zeolite at a liquid fuel flow rate of 10.6 g/hr. The

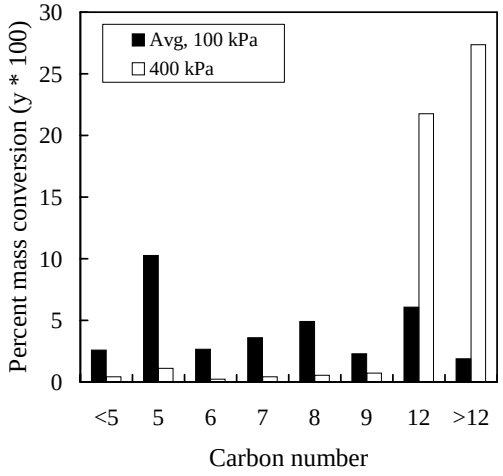

Fig. 21 Overall average product composition to determine effect of system pressure with HY zeolite at a fuel flow rate of 2.3 g/hr. The C_{10} species are omitted for clarity.

mole balance data appear in Fig. 22 for five reactor temperatures between 250°C and 500°C. As the reactor temperature decreases, the mole ratio decreases resulting in a decrease in the conversion of JP-10 into smaller products (Fig. 23).

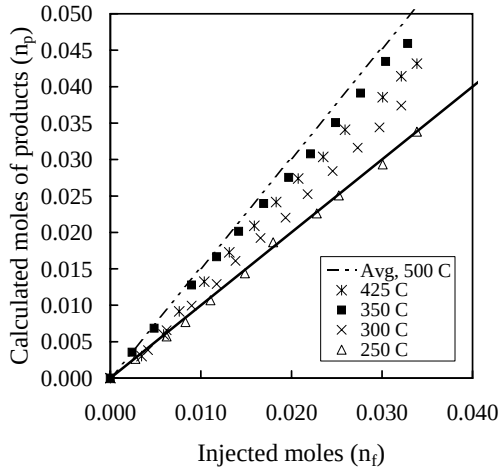

Fig. 22 Comparison of moles of product to moles of injected JP-10 in a system with HY zeolite at different reactor temperatures. Fuel flow rate is 10.6 g/hr.

The overall averaged product distributions for the multiple samples at each reactor temperature appear in Fig. 24.

The overall average conversion as a function of the reactor temperature appears in Table 8.

Average molar mass of products

The mole ratio as a function of the average mass conversion fraction is plotted in Fig. 25. The results show reasonable agreement with the simple model of a constant product average molar mass and indicate a reasonable correlation between observed mass con-

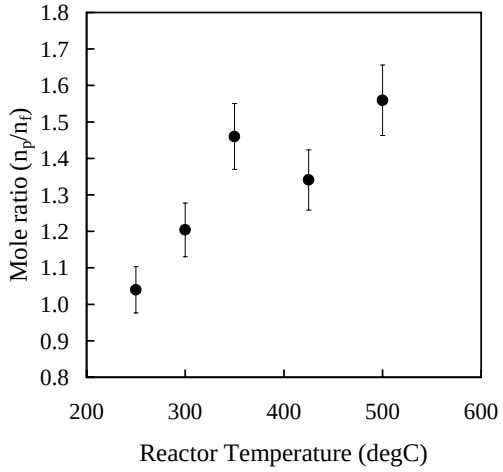

Fig. 23 Mole ratio data for reactor temperatures between 250 and 500°C. Fuel flow rate is 10.6 g/hr.

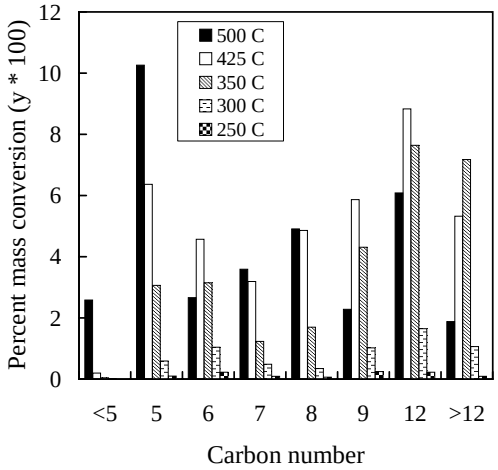

Fig. 24 Averaged product distributions for tests with HY zeolite and different reactor temperatures. The C_{10} species are omitted for clarity.

Temperature (°C)	mole ratio	% conversion
500	1.70	34
425	1.29	39
350	1.41	28
300	1.15	6
250	0.99	1

Table 8 Effect of reactor temperature on catalytic cracking tests with HY zeolite at a fuel flow rate of 10.6 g/hr.

version fraction and molar ratio. Trial 17 (Fig. 12) from the dataset is not visible on this plot because the results are so extreme. We conclude that this point is suspect and should not be used in the overall correlation process. Also, the datasets at the reactor temperature of 250°C and at a system pressure of 400 kPa were not included since JP-10 conversion was minimal as denoted by mole ratios of 1.0. These three conditions are set aside and the remainder of the data

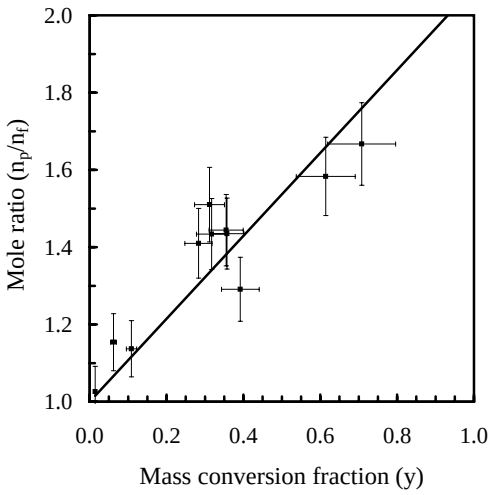

Fig. 25 Measured mole ratio n_p/n_f as a function of the mass conversion fraction y for the catalytic cracking tests.

has been considered as acceptable. The estimated uncertainty in the mole ratio of the acceptable datasets is ±6.4% and the uncertainty in the average percent mass conversion is ±12.5%.

The acceptable data can be fit to a line through the origin to obtain a slope of 1.07 with a regression coefficient of 0.75. Using the analysis of the mass balance calculations, the average molar mass of the products is estimated to be $0.48 \cdot 136$ g/mol or 65 ± 11 g/mol. The uncertainty in $\mathcal{W}_p$ is estimated to be ±17%. Thus, the average number of carbon atoms is 4.8 ± 0.8 assuming a H/C ratio of 1.6. This is reasonable considering the actual distribution of product species and the expectation that breaking the JP-10 rings to form C_5 and C_6 species is the initial path of decomposition under these conditions.

Pre-mixed partial oxidation experiments

Experiments were conducted to determine the feasibility of creating partial oxidation products by using pre-mixed combustion. A series of experiments was carried out in an explosion vessel with mixtures of JP-10 and air. An initial burn of a rich mixture was used to create the partial oxidation products. These products were allowed to cool, air was added to create a stoichiometric mixture, and a second burn was performed. Pressure measurements, high-speed video schlieren, and ideal thermodynamic computations were used to characterize the mixtures. This section of the report describes the experimental facility, the test procedure, results, and analyses of the data.

Experimental facility and procedure

The experiments were carried out in an 11.25 liter explosion vessel, shown in Fig. 26 without the surrounding insulation. The vessel was equipped with an

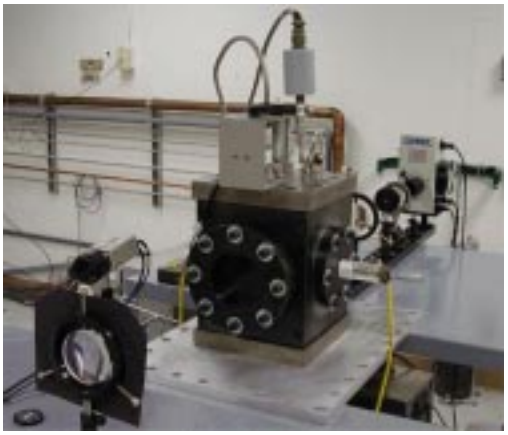

Fig. 26 Constant volume combustion vessel for pre-mixed partial oxidation experiments.

Endevco 8530B-200 pressure transducer, thermocouple, two-sided optical access for flame visualization, and a spark ignition system consisting of a capacitor discharge system and two electrodes. The facility was heated to an average of 380 K to vaporize the liquid JP-10 that was injected into the vessel through a self-sealing septum with a 1-cc syringe. A schlieren system was used to visualize the combustion fronts. The images were recorded on a Phantom IV digital camera at 512×512 resolution and 1000 frames/s. The schlieren video was used to determine the flame geometry and speed, and to verify flammability limits.

The test procedure began by evacuating the vessel and gas handling system with the vacuum pump. Liquid JP-10 was injected into the vessel to achieve a partial pressure of 1.4 kPa. Oxygen and nitrogen were then added to the vessel by the method of partial pressures (Table 9) to obtain the desired equivalence ratio.

$$\phi C_{10}H_{16} + 14(O_2 + 3.76N_2) \qquad (10)$$

ϕ	P_{JP-10} (kPa)	P_{O_2} (kPa)	P_{N_2} (kPa)	P_1 (kPa)
1	1.4	19.9	74.7	96
1.5	1.4	13.1	49.4	64
2	1.4	9.8	36.8	48
2.5	1.4	7.9	29.7	39
3	1.4	6.6	24.9	33
3.5	1.4	5.8	21.8	29
4	1.4	5.0	18.6	25
4.5	1.4	4.3	16.3	22
5	1.4	3.9	14.7	20

Table 9 Partial pressures of the first burn's initial mixture for varying equivalence ratios.

A fan stirred the mixture for five minutes to ensure mixture homogeneity. A LabView program was used to synchronize ignition with recording the pressure signals and the schlieren images.

After combustion, the products quickly cooled (<2 min) to the vessel temperature and the final pressure of the products $(P_p)_1$ was recorded. Additional oxygen and nitrogen were then added to achieve an equivalent stoichiometric mixture at 100 kPa and 380 K. The amount of air added to the mixture was

$$(\phi - 1)14(O_2 + 3.76N_2) \ . \qquad (11)$$

The mixture was again stirred and the initial pressure P_2 recorded before the second burn was completed. Pressure histories and schlieren video were recorded.

Pressure and product composition results

The recorded pressure histories for the first burn appear in Fig. 27 and 28. As the equivalence ratio increases and the mixture becomes increasingly richer, the maximum pressure of the first burn decreases. The flame develops very slowly and then is observed to extinguish in the schlieren images for the case of ϕ equal to 5 which explains the pressure rise of only 8 kPa.

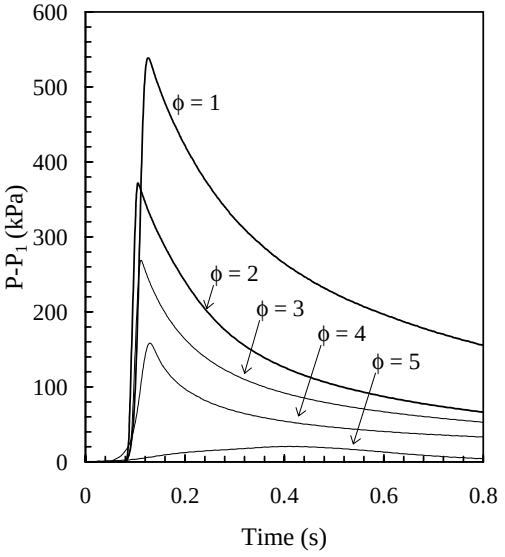

Fig. 27 Pressure histories of the first burn for ϕ equal to 1, 2, 3, 4, and 5.

Equilibrium predictions of mole concentrations and pressures for the first burn were made with STANJAN.[30] Adiabatic, constant volume, complete-combustion calculations were performed for each equivalence ratio at an initial temperature of 380 K and at initial pressures P_1 corresponding to the experimental conditions. The numbers of moles have been normalized by the initial moles of JP-10.

$$C_{10}H_{16} + n(O_2 + 3.76N_2) \qquad (12)$$

where n is $14/\phi$. Comparison between the equilibrium predictions and experimental values of $\Delta P_1 = (P_{max})_1 - P_1$ appears in Fig. 29. Using the ideal gas law with the first law of thermodynamics, the maximum pressure rise during the combustion event can be

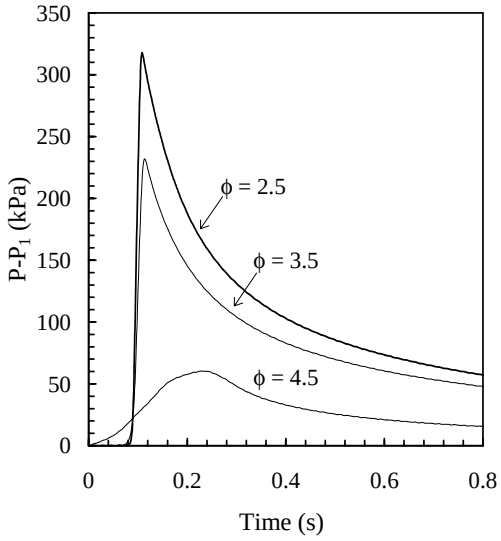

Fig. 28 Pressure histories of the first burn for ϕ equal to 2.5, 3.5, and 4.5.

related to the equivalent chemical energy release Q of the mixture.

$$Q = \frac{P_{max} - P_1}{(\gamma - 1)V} \qquad (13)$$

As the equivalence ratio ϕ is increased, the effective

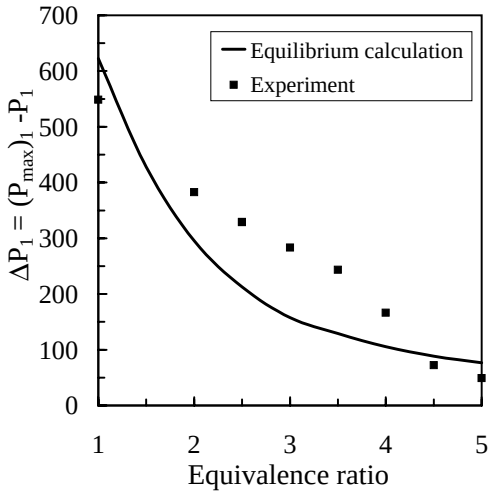

Fig. 29 Equilibrium predictions and experimental data for the peak pressure rise in the first burn ΔP_1 as a function of equivalence ratio.

energy release Q decreases since the C and H atoms are only partially oxidized.

The corresponding normalized moles of products for the first burn of JP-10 and air at different equivalence ratios appear in Fig. 30. At the stoichiometric condition (ϕ=1), the approximate reaction predicted by the equilibrium calculations is

$$C_{10}H_{16} + 14(O_2 + 3.76N_2) \rightarrow 7.8CO_2 + 7.4H_2O + 2.2CO + 52.64N_2 + \text{traces}(O_2, H_2) \ . \qquad (14)$$

All of the fuel is oxidized completely to major products, mostly CO_2 and H_2O. At an equivalence ratio of

2.5, the approximate reaction predicted by the equilibrium calculation is

$$C_{10}H_{16}+5.6(O_2+3.76N_2) \rightarrow 9.6CO+7H_2 + 21N_2+\text{traces}(CO_2,H_2O)\ . \qquad (15)$$

The fuel is oxidized to only CO and H_2. There is not enough O_2 to create H_2O or CO_2 for $\phi \geq 2.5$. At an equivalence ratio of 4, an approximate reaction is

$$C_{10}H_{16}+3.5(O_2+3.76N_2) \rightarrow 7CO+4H_2 + 13N_2+1.6CH_4+\text{traces}(C_2H_x)\ . \qquad (16)$$

The excess fuel forms CH_4 and trace amounts of higher hydrocarbons. The H_2, CO, CH_4, and other hydrocarbons act as the fuel for the second burn when air is added to the system.

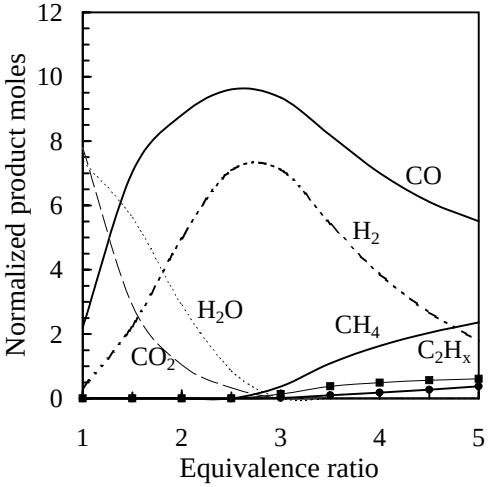

Fig. 30 Normalized moles of products for $C_{10}H_{16}$ + n(O_2 + 3.76N_2) as a function of the equivalence ratio. N_2 moles are omitted for clarity. Equilibrium computations under adiabatic, constant volume complete combustion conditions.

After the first burn with JP-10 and air, the products were allowed to cool to the vessel temperature of 380 K. The ratio of initial and final pressures is equal to the ratio of product moles to the reactant moles by the ideal gas law since the vessel volume is constant.

$$\frac{(P_p)_1}{P_1} = \left(\frac{(n_p)_1 RT}{V}\right)\left(\frac{V}{n_1 RT}\right) = \frac{(n_p)_1}{n_1} \qquad (17)$$

Two predictions of the cooling process to the initial temperature of 380 K were conducted with STANJAN. The equilibrium case calculates the concentrations assuming the reactions progress extremely quickly and the composition is at equilibrium at 380 K. The frozen case calculates the concentrations assuming the reactions progress extremely slowly and the composition is fixed at that found for the adiabatic conditions associated with the first burn (Fig. 30). The two predictions are compared with the experimental data in Fig. 31.

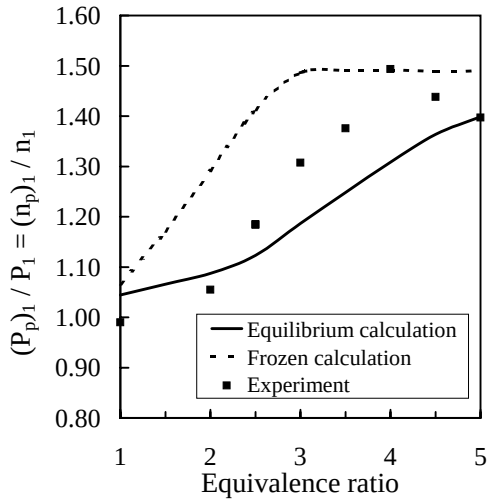

Fig. 31 Predicted and experimental values of $(P_p)_1/P_1$ as a function of equivalence ratio.

The experimental data generally lie between the two limiting predictions of equilibrium and frozen product concentrations. The dependence of maximum temperature (Fig. 32) during the first burn (as predicted by the equilibrium calculation) helps explain the trend of the data shown in Fig. 31. The peak temperature

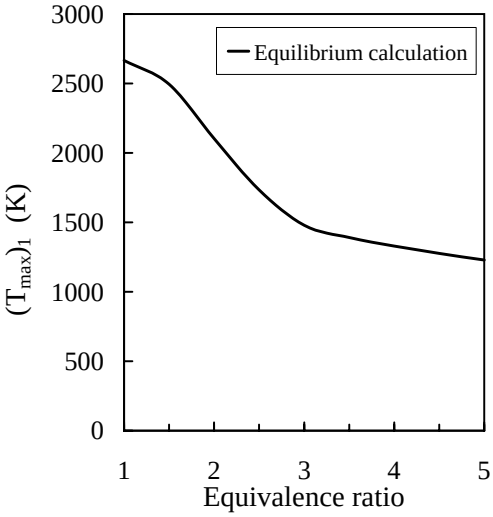

Fig. 32 Equilibrium predictions of the maximum temperature during the first burn as a function of equivalence ratio. Adiabatic, constant volume, complete combustion process.

decreases with increasing equivalence ratio. For $1 < \phi < 2.5$, the temperature is sufficiently high that the reactions in the products proceed rapidly before heat transfer to the vessel walls reduces the gas temperature and the chemical reactions cease. For these cases, the equilibrium model appears to be appropriate. As the equivalence ratio increases, $\phi > 2.5$, the peak temperature drops and the rate of the chemical reactions decreases. The reaction apparently does not have time to take place before the gas cools to the vessel temperature. For these cases, the frozen model appears to be

appropriate.

For equivalence ratios greater than 4, combustion produces a significant amount of soot, decreasing the final pressure relative to the predictions which do not account for the formation of carbon-containing solids. In addition, incomplete combustion occurs, resulting in a lower pressure rise in comparison to the complete combustion prediction. For equivalence ratios greater than 5, the combustion could not be initiated. This is consistent with the very low pressure rise observed at $\phi = 5$ (Fig. 27).

The normalized product distributions for the cool gas assuming equilibrium composition appear in Fig. 33. For equivalence ratios near stoichiometric, the products are composed almost entirely of H_2O and CO_2. For the higher equivalence ratios, the products are composed almost entirely of CO and CH_4. The product distribution for the cooled gas assuming

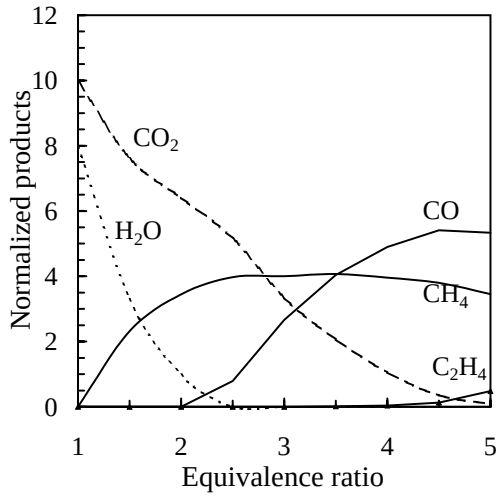

Fig. 33 Normalized moles of cooled products calculated with equilibrium concentrations as a function of the first burn equivalence ratio. N_2 moles are omitted for clarity.

a frozen composition is the same as in Fig. 30.

After the products have cooled to the initial temperature of the vessel, oxygen and nitrogen are added to form an equivalent stoichiometric mixture. The mixture is ignited and the pressure histories are recorded. The initial pressure for the second burn after the addition of the oxygen and nitrogen is approximately 100 kPa. The recorded pressure histories for the second burn appear in Fig. 34. As the first burn equivalence ratio increases, the maximum pressure of the second burn at an equivalent stoichiometric condition increases. This is a result of the partial oxidation products (CO, H_2, and hydrocarbons) of the first burn now being fully oxidized by the added oxygen. No second burn was achieved for values of ϕ less than 2.5 since only a very small fraction of the products of the first burn are incompletely oxidized. In these cases, the mixtures are too lean to be flammable.

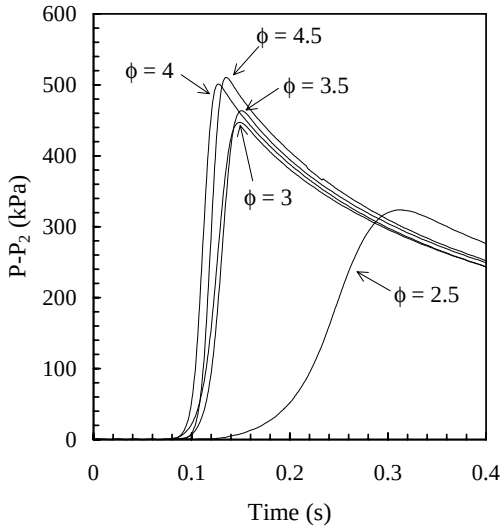

Fig. 34 Pressure histories of the second burn for ϕ equal to 2.5, 3, 3.5, 4, and 4.5.

Adiabatic, constant volume explosion pressure and species computations were carried out with STANJAN for the second burn. These computations were done using both frozen and equilibrium compositions resulting from the first burn. The predictions are compared with the experimental data for ΔP_2 in Fig. 35. The horizontal lines in the figure correspond to the maximum pressure rise realized for the experimental data (548 kPa) and the predicted value (615 kPa) for stoichiometric combustion of JP-10 and air at 100 kPa and 380 K. In both the predicted and experimental cases, the maximum pressure rise obtained by combusting products of rich JP-10 combustion in air is less than the pressure rise obtained by combusting a stoichiometric mixture of JP-10 in air.

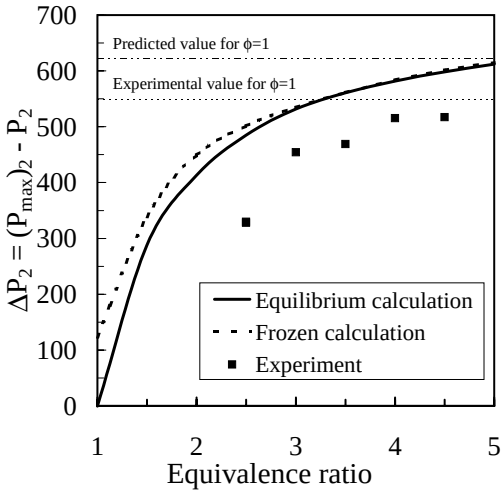

Fig. 35 Predicted and experimental values of ΔP_2 as a function of equivalence ratio.

We define an effectiveness factor ϵ for the second

burn

$$\epsilon = \frac{(\Delta P)_2}{(\Delta P_1)_{\phi=1}} \ . \tag{18}$$

The effectiveness is a measure of chemical energy conversion in the second burn as compared to that obtained by the stoichiometric combustion of JP-10 in air at the same initial conditions. The effectiveness is zero for cases in which no first ($\phi \geq 5$) or second ($\phi < 2.5$) combustion event occurred. In both the experimental data and predictions based on equilibrium calculations, the effectiveness is always less than 1 implying that partial oxidation releases less energy than would be released if JP-10 in air at stoichiometric conditions was burned directly (Fig. 36).

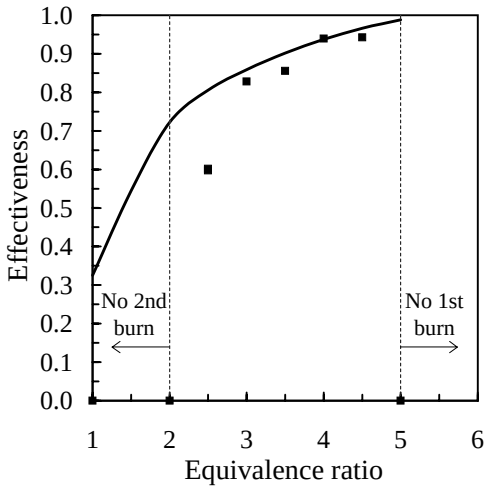

Fig. 36 Predicted and experimental effectiveness values as a function of the first burn equivalence ratio.

The equilibrium product distributions have been computed for the second burn. The case of starting with the frozen composition (Fig. 30) for the first burn is shown in Fig. 37. The case of starting with the equilibrium composition (Fig. 33) for the first burn is shown in Fig. 38. In both cases, the results have been normalized to one mole of fuel and the major products are CO_2, H_2, and CO.

A decrease in the product concentrations of CO_2 and H_2O occurs as the first burn equivalence ratio increases (Fig. 38 and 37). The maximum temperature of the second burn increases with equivalence ratio as shown in Fig. 39. Thus, the decrease in CO_2 and H_2O can be attributed to dissociation at the higher temperatures. The slightly higher temperature for the reaction with the frozen reactants results in more dissociation as compared to the reactants from the equilibrium case.

Schlieren images visualizing the flame front at equivalence ratios of 1, 3, and 5 were recorded. Successive images were used to determine the flame velocity as a function of the changing radius over time. The laminar burning speed was derived from these measurements as described in detail in Cooper and Shepherd.[9] The laminar burning speed of stoichiometric JP-10 and air mixtures at 100 kPa and 380 K was found to be about 64 cm/s.[9] This value is greater than the measurements of Parsinejad and Metghalchi[31] who measured a burning speed of approximately 30 cm/s at initial conditions of 1 atm and 460 K.

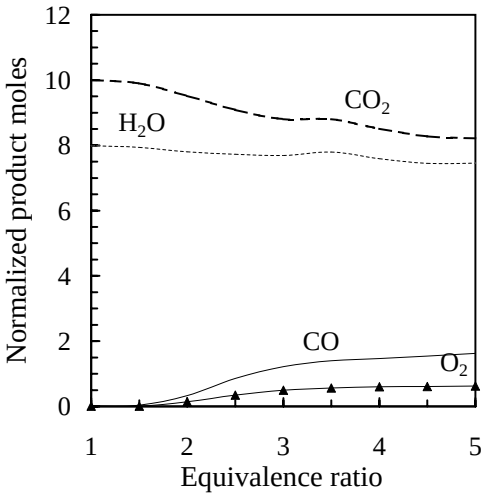

Fig. 37 Normalized product moles of second burn with reactants calculated using frozen chemistry as a function of the first burn equivalence ratio. N_2 moles are omitted for clarity.

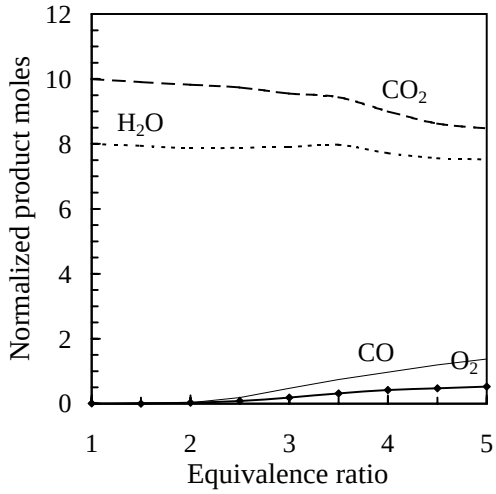

Fig. 38 Normalized product moles of second burn with reactants calculated using equilibrium concentrations as a function of the first burn equivalence ratio. N_2 moles are omitted for clarity.

Conclusions

Three mechanisms of JP-10 hydrocarbon cracking have been investigated. Product compositions and conversion percentages were quantified for thermal decomposition and catalytic cracking experiments in a benchtop reactor. Pre-mixed partial oxidation experiments were conducted in an explosion vessel and maximum pressures were measured in addition to quantifiying a burning efficiency.

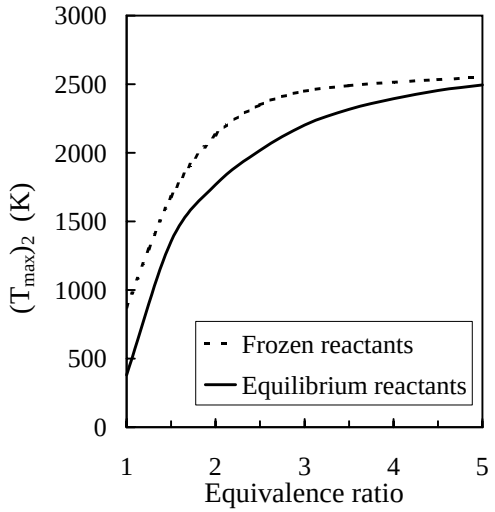

Fig. 39 Predictions of the maximum temperature during the second burn as a function of equivalence ratio.

Thermal cracking experiments at a reactor temperature of 500°C and liquid fuel flow rates between 2.3 and 10.6 g/hr yielded conversion ratios of approximately 3% and less. Small increases, less than a few tenths of a percent, were observed in the C_5 and C_6 amounts. The mechanism of thermal cracking at 500°C appears to have no significant benefit for increased efficiency of detonation initiation. Thermal reactions will likely increase for reactor temperatures greater than 500°C, however, it remains to be seen whether conversion ratios on the order of the catalytic cracking reactions could ever be reached by thermal cracking alone.

The effect of the liquid fuel flow rate on JP-10 conversion was studied in both the thermal and catalytic cracking tests. In both cases, the amount of JP-10 conversion increased as the liquid fuel flow rate decreased. However, the changes were modest and the average conversion was found to increase less than 10% in the most extreme case. Because of the increased residence time of the molecules in the heated reactor plumbing at the lower flow rates, chemical reactions had more time to initiate and for surface reactions to occur. Due to the size of our system and the fuel pump capabilities, testing at lower flow rates was not easily achieved without significant repeatibility issues. Testing at even lower flow rates may observe higher conversion ratios, but coking is likely to become more of a problem since deposit formation is accelerated as the Reynolds number decreases.

Three zeolites (HY, USY, and Beta) were tested to determine their effect on the conversion ratio. HY is known as a large-pore zeolite commonly used in heavy oil cracking, while USY is a modified version of the Y zeolite designed to be more resistant to coke deposits. Beta has a larger range of pore dimensions suggesting it might be able to produce a greater variety of cracked products. The mole balance results were similar for HY and Beta, while USY was significantly lower. The USY zeolite was not observed to have a significant reduction in coking as compared to the others. It seems that none of these tested zeolites are optimal for hydrocarbon cracking with JP-10 due to the rapid deactivation by coke deposits and relatively low conversion ratios.

The effect of elevated system pressure on cracking was measured by applying a backpressure to the accumulator in addition to pressurizing the system with nitrogen to approximately 400 kPa. The movement of the accumulator position was significantly reduced for the case at 400 kPa as compared with the 100 kPa case as denoted by the reduced mole ratio. However, the GC analysis observed a greater conversion of JP-10 into higher-molecular-weight components.

A series of catalytic cracking tests was completed with the HY zeolite as a function of reactor temperature since chemical reactions are known to have a strong dependence on temperature. The conversion percent and mole balance both increase as the temperature in the reactor increases.

A comparison between the mole ratio and mass conversion fraction for the thermal cracking results yielded too much variability and an average molar mass of the products could not be determined. For catalytic cracking, however, the measured mole ratio was found to be an approximately linear function of the mass conversion fraction (Fig. 25). This indicated that the average molar mass of the products is approximately constant. Using the mass balance and mole balance analysis for the overall reaction, the average molar mass of the products is estimated to be 65 ± 11 g/mol. Assuming that all the atoms are in a single notional molecule, the average number of carbon atoms is 4.8 ± 0.8 for an H/C ratio of 1.6.

Experiments were carried out in an explosion vessel to examine the feasibility of creating partial oxidation products with rich pre-mixed combustion. Mixtures of JP-10 and air could be combusted up to an equivalence ratio of 5. The rich flammability limit appears to be at about 5. The combustion products of rich mixtures with $\phi > 2$ appear to be consistent with the products predicted by a frozen cooling of the adiabatic, equilibrium, constant volume explosion products.

For equivalence ratios between 2.5 and 4.5, it was possible to add a stoichiometric amount of air after the first burn and carry out a second burn. The peak pressure obtained in the second burn was consistent with equilibrium predictions assuming frozen product composition of the first burn. The peak pressure rise of the second burn was an increasing function of the first burn equivalence ratio and reaches a maximum value of about 95% of the stoichiometric peak pressure rise at an initial equivalence ratio of 4 to 4.5. We conclude that from an energetics point of view, partial oxidation should be carried out an equivalence ratio that is as

high as possible while avoiding soot production. Soot production was evident in the present experiments as the equivalence ratio approached 5. Other properties such as flame speed, expansion ratio, and detonation cell size need to be examined to further constrain the choice of equivalence ratio.

Acknowledgement

This work was carried out under P.O. No. 00-592 for Advanced Projects Research, Inc. under AF contract F04611-99-C-0017. Contract administration, mechanical design and fabrication of two components of the facility: the reactor heater and accumulator, were carried out by Advanced Projects Research, Inc. Key participants from APRI included Toby Rossmann, Jay Marsh, Kevin Moore, and Tom Sobota.

We acknowledge Kathia Devouge for her preliminary design work. Special thanks to Nathan Dalleska, Director of the Environmental Analysis Center at Caltech, for his immensely valuable lessons on the theory and operation of the gas chromatograph. Prof. Mark Davis of Chemical Engineering at Caltech and members of his research group were very helpful with sharing their expertise in zeolite chemistry. In particular, we thank Andrea Wight, Ph.D. student in Chemical Engineering at Caltech, for providing not only many zeolite samples and use of her chemical laboratory but also many helpful discussions on zeolite structure, preparation, and handling procedures. We thank Daniel Lieberman for his contributions to the pre-mixed partial oxidation experiments.

References

[1]Austin, J. M. and Shepherd, J. E., "Detonation in Hydrocarbon Fuel Blends," *Combustion and Flame*, Vol. 132, No. 1-2, 2002, pp. 73–90.

[2]Hitch, B., "The Effect of Autoignition-Promoting Additives on Deflagration-to-Detonation Transition," 38th AIAA/ASME/SAE/ASEE Joint Propulsion Conference and Exhibit, July 7–10, 2002, Indianapolis, IN, AIAA 2002–3719.

[3]Akbar, R., Thibault, P. A., Harris, P. G., Lussier, L. S., Zhang, F., Murray, S. B., and Gerrard, K., "Detonation Properties of Unsensitized and Sensitized JP-10 and Jet-A Fuels in Air for Pulse Detonation Engines," 36th AIAA/ASME/SAE/ASEE Joint Propulsion Conference and Exhibit, July 16–19, 2000, Huntsville, AL, AIAA 2000–3592.

[4]Zhang, F., Murray, S. B., and Gerrard, K. B., "JP-10 Vapour Detonation at Elevated Pressures and Temperatures," 18th ICDERS, Seattle, WA, July 29 – August 3, 2001.

[5]Davidson, D. F., Horning, D. C., Oehlschlaeger, M. A., and Hanson, R. K., "The Decomposition Products of JP-10," 37th AIAA/ASME/SAE/ASEE Joint Propulsion Conference and Exhibit, July 8–11, 2001, Salt Lake City, UT, AIAA 2001–3707.

[6]Li, S. C., Varatharajan, B., and Williams, F. A., "The Chemistry of JP-10 Ignition," 39th AIAA Aerospace Sciences Meeting and Exhibit, January 8–11, 2001, Reno, NV, AIAA 2001–1074.

[7]Edwards, T., ""Kerosene" Fuels for Aerospace Propulsion – Composition and Properties," 38th AIAA/ASME/SAE/ASEE Joint Propulsion Conference and Exhibit, July 7–10, 2001, Indianapolis, IN, AIAA 2002–3874.

[8]Schauer, F., Stutrud, J., and Bradley, R., "Detonation Initiation Studies and Performance Results for Pulsed Detonation Engines," 39th AIAA Aerospace Sciences Meeting and Exhibit, January 8–11, 2001, Reno, NV, AIAA 2001-1129.

[9]Cooper, M. and Shepherd, J. E., "Thermal and Catalytic Cracking of JP-10 for Pulse Detonation Engine Applications," GALCIT Report FM2002.002, Graduate Aeronautical Laboratories, California Institute of Technology, Pasadena, CA 91125, 2002.

[10]Woodrow, J. E., "The Laboratory Characterization of Jet Fuel Vapor and Liquid," *Energy and Fuels*, Vol. 17, No. 1, Jan.–Feb. 2003, pp. 216–224.

[11]Lopes, J. M., Lemos, F., Ribeiro, F. R., and Derouane, E. G., "A comparison of the catalytic properties of SAPO-37 and HY zeolite in the cracking of n-heptane and 2,2,4-trimethylpentane," *Zeolite Chemistry and Catalysis*, edited by P. A. Jacobs, Elsevier Science Publishers, B.V., Amsterdam, 1991, pp. 365–371.

[12]Townsend, A. T. and Abbot, J., *Catalytic cracking of tetralin on HY zeolite*, Vol. 90 of *Applied Catalysis A: General*, Elseview Science Publishers, B.V., Amsterdam, 1991, pp. 97–115.

[13]Spadaccini, L. J., Sobel, D. R., and Huang, H., "Deposit Formation and Mitigation in Aircraft Fuels," *Journal of Engineering for Gas Turbines and Power*, Vol. 123, October 2001, pp. 741–746.

[14]Abbot, J. and Wojciechowski, B. W., "Catalytic Reactions of n-hexane on HY Zeolite," *The Canadian Journal of Chemical Engineering*, Vol. 66, October 1988, pp. 825–829.

[15]Pickard, J. A. and Jones, E. G., "Kinetics of the Autoxidation of a Jet-A Fuel," *Energy and Fuels*, Vol. 10, No. 5, Sep.–Oct. 1996, pp. 1074–1077.

[16]Green, R. J., Nakra, S., and Anderson, S. L., "Breakdown Behavior of Fuels for Pulse Detonation Engines," *Fourteenth ONR Propulsion Meeting*, edited by G. D. Roy and F. Mashayek, Department of Mechanical & Industrial Engineering, University of Illinois at Chicago, Chicago, August 2001, pp. 213–217.

[17]Edwards, T., "Storable Fuels and Connected Issues of Hypersonic Flight," *Future Aerospace Technology in the Service of the Alliance: Sustained Hypersonic Flight*, NATO RTO, December 1997, AGARD-CP-600-03-Vol 3.

[18]Olah, G. A. and Molnar, A., *Hydrocarbon Chemistry*, John Wiley and Sons, Inc., New York, NY, 1995.

[19]Dyer, A., *An Introduction to Zeolite Molecular Sieves*, John Wiley and Sons, Inc., New York, NY, 1988.

[20]van Santen, R. A. and Niemantsverdriet, J. W., *Chemical Kinetics and Catalysis*, Plenum Press, NY, 1995.

[21]Meier, W. M. and Olson, D. H., *Atlas of Zeolite Structure Types*, Butterworth-Heinemann, London, 3rd ed., 1992.

[22]Chang, C. D., *Hydrocarbons from Methanol*, Marcel Dekker, Inc., NY, 1983.

[23]Honna, K., Sato, K., Araki, Y., Miki, Y., Matsubayashi, N., and Shimada, H., "HY zeolite-based catalyst for hydrocracking heavy oils," *Hydrotreatment and Hydrocracking of Oil Fractions*, edited by B. Delmon, G. F. Froment, and P. Grange, Elsevier Science, B.V., Amsterdam, 1999, pp. 427–430.

[24]Dwyer, J., Dewing, J., Karim, K., Ojo, A. F., Garforth, A. A., and Rawlence, D. J., "Hydrocarbon Transformations over Analogues and Derivatives of Zeolite Y," *Zeolite Chemistry and Catalysis*, edited by P. A. Jacobs, Elsevier Science Publishers, B.V., Amsterdam, 1991, pp. 1–23.

[25]Paal, Z. and Xu, X. L., "Reactions of n-Hexane over Pt-HZSM-5 Catalyst," *Studies in Surface Science and Catalysis*, edited by H. K. Beyer, H. G. Karge, I. Kiricsi, and J. B. Nagy, No. 94 in Catalysis by Microporous Materials, Elsevier Science, B. V., Amsterdam, 1995, pp. 590–597.

[26]Sobel, D. R. and Spadaccini, L. J., "Hydrocarbon Fuel Cooling Technologies for Advanced Propulsion," *Journal of Engineering for Gas Turbines and Power*, Vol. 119, April 1997, pp. 344–351.

[27]H. Huang, D. R. S. and Spadaccini, L. J., "Endothermic Heat-Sink of Hydrocarbon Fuels for Scramjet Cooling," 38th AIAA/ASME/SAE/ASEE Joint Propulsion Conference and Exhibit, July 7–10, 2001, Indianapolis, IN, AIAA 2002–3871.

[28]Lander, H. and Nixon, A. C., "Endothermic Fuels for Hypersonic Vehicles," *Journal of Aircraft*, Vol. 8, No. 4, 1971, pp. 200–207.

[29]Chin, J. S. and Lefebvre, A. H., "Influence on Flow Conditions on Deposits From Heated Hydrocarbon Fuels," *Journal of Engineering for Gas Turbines and Power*, Vol. 115, July 1993, pp. 433–438.

[30]Reynolds, W. C., "The Element Potential Method for Chemical Equilibrium Analysis: Implementation in the Interactive Program STANJAN, Version 3," Tech. rep., Dept. of Mechanical Engineering, Stanford University, Stanford, CA, January 1986.

[31]Parsinejad, F. and Metghalchi, H., "Burning Speed and Autoignition Characteristics of JP10-Air Mixtures," *Sixteenth ONR Propulsion Meeting*, edited by G. D. Roy and M. A. Gundersen, Department of Electrical Engineering – Electrophysics, University of Southern California, Los Angeles, June 2003, pp. 49–54.